American Mineralogist, Volume 96, pages 1495–1502, 2011

The compression pathway of quartz

Richard M. Thompson,[1,*] Robert T. Downs,[1] and Przemyslaw Dera[2]

[1]Department of Geosciences, University of Arizona, Tucson, Arizona 85721-0077, U.S.A.
[2]GSECARS, University of Chicago, Building 434A, 9700 South Cass Avenue, Argonne, Illinois 60439, U.S.A.

Abstract

The structure of quartz over the temperature domain (298 K, 1078 K) and pressure domain (0 GPa, 20.25 GPa) is compared to the following three hypothetical quartz crystals: (1) Ideal α-quartz with perfectly regular tetrahedra and the same volume and Si-O-Si angle as its observed equivalent (ideal β-quartz has Si-O-Si angle fixed at 155.6°). (2) Model α-quartz with the same Si-O-Si angle and cell parameters as its observed equivalent, derived from ideal by altering the axial ratio. (3) BCC quartz with a perfectly body-centered cubic arrangement of oxygen anions and the same volume as its observed equivalent.

Comparison of experimental data recorded in the literature for quartz with these hypothetical crystal structures shows that quartz becomes more ideal as temperature increases, more BCC as pressure increases, and that model quartz is a very good representation of observed quartz under all conditions. This is consistent with the hypothesis that quartz compresses through Si-O-Si angle-bending, which is resisted by anion-anion repulsion resulting in increasing distortion of the *c*/*a* axial ratio from ideal as temperature decreases and/or pressure increases.

Keywords: Crystal structure, ideal quartz, model quartz, BCC quartz, high-pressure studies, high-temperature studies, Brazil law twins, Dauphiné twin

Introduction

The important Earth material quartz may constitute as much as 20% of the upper continental crust (Taylor and McLennan 1985). Quartz is composed solely of corner-sharing SiO_4 silica tetrahedra, a primary building block of many of the Earth's crustal and mantle minerals, lunar, and Martian minerals, and meteoritic minerals (Deer et al. 1978). Quartz is therefore an outstanding model material for investigating the response of this fundamental structural unit to changes in *P*, *T*, and *x*. These facts have spawned a vast literature of experimental and theoretical studies of quartz at ambient and non-ambient conditions. Thompson and Downs (2010) presented a comprehensive review of the literature on the behavior of quartz at high pressure.

Investigations into the behavior of quartz at high pressure have revealed an anomalous distortion in the silicate tetrahedron with pressure not typically seen in other silicates. Traditionally, this distortion has been considered a compression mechanism (cf. Levien et al. 1980). Levien et al. (1980) claimed that, "Because a regular tetrahedron occupies the greatest volume for any tetrahedron of that average size, as it distorts its volume must decrease." However, between 0.59 and 20.25 GPa (Dera et al. in prep), unit-cell volume in quartz decreases by 21%, while Si tetrahedral volume decreases by only 1%. Over this same pressure domain, tetrahedral angle variance (Robinson et al. 1971), a traditional measure of tetrahedral distortion, increases from 0.72 to 21.24. Thus, the distortion in the Si tetrahedron is not contributing to the compression of the bulk crystal and the tetrahedron is actually much more resistant to compression than the unoccupied tetrahedral voids around it (Thompson and Downs 2010). Implicit in the above quote (Levien et al. 1980) is the idea that an atomic-scale behavior must contribute to the compression of a crystal to be considered a compression mechanism and Thompson and Downs (2010) explicitly adopted this definition.

Thompson and Downs (2010) compared observed quartz with a hypothetical high-pressure "endpoint" structure that has a perfectly body-centered cubic (BCC) arrangement of oxygen anions and confirmed the conclusion of Sowa (1988) that quartz becomes more like this structure with pressure. They analyzed the individual responses of the Si tetrahedron and the seven crystallographically non-equivalent unoccupied tetrahedral sites to increases in pressure. They reached the conclusion that the distortion in the Si tetrahedron with pressure was due to anion-anion repulsion and was actually resisting compression, and suggested that it should not be called a compression mechanism.

An important prior result that Thompson and Downs (2010) incorporated into their argument was the Rigid Unit Mode (RUM) theory conclusion that the Si-O-Si angle in quartz can theoretically change without inducing distortion in the silica tetrahedra, implying that the α-quartz structure has no intrinsic geometrical constraint creating the distortion during compression [see Dove et al. (1995) for a paper specifically addressing RUM theory and quartz; Ross (2000) for an excellent review of RUM theory applied to silicates with numerous references]. Smith (1963) derived some geometrical constraints that must be satisfied for a quartz structure to contain regular tetrahedra. Megaw (1973) correctly derived the structure of a hypothetical β-quartz with regular tetrahedra and a very good approximation of α-quartz with regular tetrahedra. Dera et al. (in prep) extended the Thompson and Downs (2010) analysis with a new

* E-mail: rmthomps@email.arizona.edu

high-pressure data set for quartz to 20.25 GPa.

The present study verifies the theoretical result that there is no inherent geometrical constraint forcing the Si tetrahedron to distort with pressure by deriving a hypothetical quartz structure with perfectly regular tetrahedra parameterized in terms of the Si-O-Si angle, θ, and the model oxygen radius, r. This hypothetical structure is hereafter referred to as "ideal quartz" and can compress by angle bending alone, without inducing any tetrahedral distortion. Figure 1 illustrates the change in volume in ideal quartz with a perfectly regular tetrahedron of fixed volume as the Si-O-Si angle decreases. The initial (largest and leftmost) volume and Si-O-Si angle equal the volume and angle for Kihara's (1990) 838 K α-quartz (the highest temperature for which α-phase structural data exists). The decrease in volume in ideal quartz is approximately equal to the decrease observed in the data sets of Kihara (1990), Glinnemann et al. (1992), and Dera et al. (in prep), and results only from Si-O-Si angle-bending. This raises the question: Why should quartz deviate from ideal at all? This paper investigates how and why observed and ideal quartz differ, extending the comparison of observed and BCC quartz of Thompson and Downs (2010) and their investigation into the origin of tetrahedral distortion in quartz with pressure.

A brief explanation of the choice of the model oxygen radius, r, as a parameter used to calculate ideal quartz structures will provide further motivation for this inquiry. The function of r is to fix the volume of a given ideal quartz structure (geometry is uniquely defined by the Si-O-Si angle). Equations for calculating ideal quartz could have been cast in terms of another parameter such as **a**, **c**, or tetrahedral volume. However, the authors have long been interested in the role of anion-anion interactions in the behavior of minerals under changing conditions of pressure, temperature, and composition. Many oxide minerals have been described as composed of a closest-packed arrangement of large oxygen anions with smaller cations in the interstitial voids (cf. Thompson and Downs 2001 and references therein), and the arrangement of oxygen atoms in quartz is distorted BCC, an ordered packing of oxygen atoms that are in contact along the diagonals of the BCC cell. In this view, the choice of the model oxygen radius as a parameter in deriving ideal crystal structures is natural as it correlates with an important physical quantity in determining the volumes of real crystals. This paper furthers our study of the role of anion-anion interactions in the behavior of quartz with temperature and pressure.

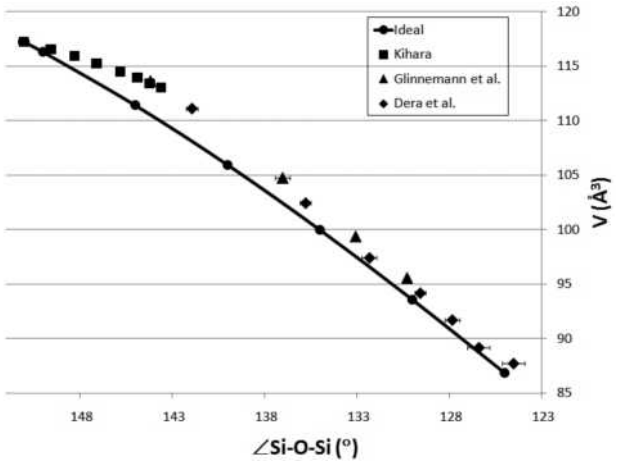

FIGURE 1. Volume vs. Si-O-Si angle in ideal and observed quartz. Ideal quartz has perfectly regular tetrahedra and in this figure is compressed by Si-O-Si angle-bending alone. Data from Kihara (1990), Glinnemann et al. (1992), and Dera et al. (in prep). Some horizontal and all vertical error bars too small to be seen.

REVIEW OF α-QUARTZ

The term "α-quartz" refers to either of two naturally occurring enantiomorphous crystal structures (called "Brazil law" twins when they occur in the same crystal), each of which can be described in one of two settings referred to as α1 and α2 (forming "Dauphiné" twins when adjacent portions of a crystal cannot be described in the same setting with a unique set of coordinate axes).

α-quartz with space group $P3_221$ and β-quartz with space group $P6_222$ are referred to as "right-handed" based on macroscopic (optical and morphological) properties, while α-quartz with space group $P3_121$ and β-quartz with space group $P6_422$ are referred to as "left-handed" (Megaw 1973). Right-handed quartz can be described as structurally left-handed because it is composed of left-handed threefold spirals of tetrahedra running parallel to **c**, but it can also be thought of as composed of right-handed double helices of tetrahedra, where a complete turn of one of the helices contains six tetrahedra.

The settings α1 and α2 can be defined in terms of their relationship to β-quartz. In the conventional β-quartz setting, there is a silicon atom at [1/2, 0, 0] bonded to an oxygen at [x, x/2, –1/6] where x is ~0.4. This oxygen atom is on a twofold axis that runs parallel to [210] (Fig. 2). Once an origin and cell have been defined for β-quartz, as it cools through the transition temperature to α-quartz, the tetrahedron containing these two atoms can either screw toward the origin (termed α1 after Young 1962) or away from it (α2) (Bragg et al. 1965). If the crystal adopts the α1 setting, the silicon atom moves from [1/2, 0, 0] toward the origin along the **a** axis, while the oxygen atoms rotate around the **a** axis in the counterclockwise direction as they, too, move toward the origin. Otherwise, the silicon atom moves away from the origin and the oxygen atoms rotate in clockwise fashion. These two possibilities create the screwing motions described

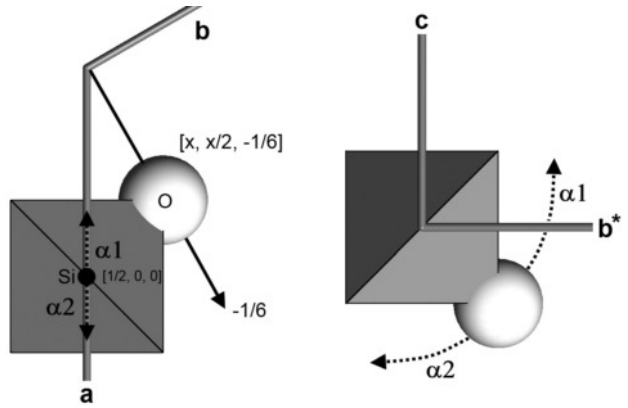

FIGURE 2. The transition from β-quartz into the α1 and α2 settings for left-handed quartz.

above. In the $\alpha1$ setting, $x_O < 2y_O$ and $x_{Si} < 1/2$; in $\alpha2$, $x_O > 2y_O$ and $x_{Si} > 1/2$. Figure 2 illustrates these two possibilities for left-handed quartz. The direction of motion of the silicon atom in the two settings is indicated by dotted arrows superimposed on the **a** axis in the left-hand side of the figure, while the rotation about **a** of the oxygen atoms is similarly illustrated on the right-hand side. This paper refers to the angle that results from the projection of the rotation angle of the tetrahedron about **a** onto the **b*c**-plane as the tetrahedral rotation angle, ϕ ($\phi = 0$ in the right side of Fig. 2, see Fig. 6). In left-handed quartz, screwing of the tetrahedron toward the origin requires a counterclockwise rotation, while right-handed quartz requires clockwise motion. The setting can be changed between $\alpha1$ and $\alpha2$ by rotating the unit cell 180° around **c**. In left-handed quartz, the $\alpha1$ setting can be also be transformed to $\alpha2$ by a 60° rotation of the unit cell and translating the origin along **c** of 2/3 of the cell edge (1/3 in right-handed quartz). When the same crystal contains two domains such that the tetrahedral rotation angle in one of the domains is in the opposite direction of those of the translationally equivalent tetrahedra in the second domain, Dauphiné twinning exists.

The twin plane for Brazil law twins is (110) (Bragg et al. 1965). Figure 3 is an illustration of a model twin created by reflecting across (110). This simple model results in a physically unrealistic planar SiO_4 group. In reality, the twin boundary must be different from this model, perhaps occurring in step-wise fashion over a volume instead of a surface, and/or containing different chemistry. With the choice of **a** and **b** illustrated in Figure 3, the unit cells for the enantiomorphs are offset by 1/3 along **c** and the $\alpha1$ setting is preserved in both enantiomorphs (equivalently, the direction of tetrahedral rotation is reversed).

Data sets for all of the hypothetical structures used in this paper are on deposit. They are all described as left-handed in the $\alpha1$ setting. Their asymmetric units have the silicon atom at approximately [1/2, 0, 0] and its bonded oxygen atom at approximately [0.4, 0.2, –1/6]. The right-handed equivalent can be derived by changing the sign of z. The following formulas allow the transformation from the $\alpha1$ setting to the $\alpha2$ setting and back:

$$x_{Si}(\alpha2) = 1 - x_{Si}(\alpha1)$$
$$x_O(\alpha2) = x_O(\alpha1)$$
$$y_O(\alpha2) = x_O(\alpha1) - y_O(\alpha1)$$
$$z_O(\alpha2) = -1/3 - z_O(\alpha1), \text{ left-handed quartz}$$
$$z_O(\alpha2) = 1/3 - z_O(\alpha1), \text{ right-handed quartz.}$$

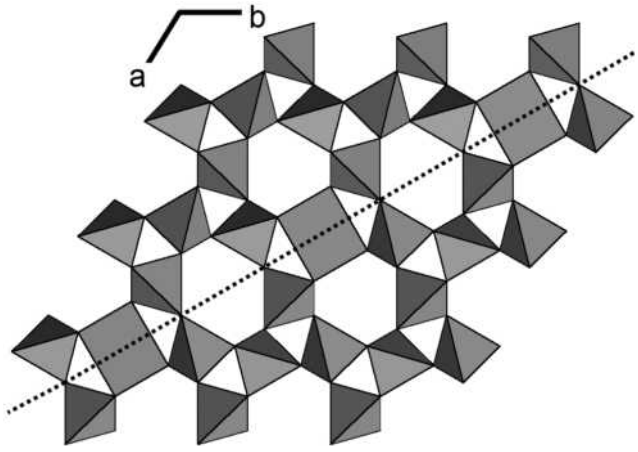

FIGURE 3. A simple model of Brazil law twins.

In the following, when a hypothetical structure is described as uniquely defined by specifying certain parameters, this means unique up to enantiomorphism.

OVERVIEW OF MODELS AND DATA

Four types of quartz structures are defined and compared in this paper—observed quartz and three hypothetical model structures: ideal quartz, model quartz, and BCC quartz. Figure 4 is a graphic comparison of observed quartz at 20.25 GPa (Dera et al. in prep) and its ideal, model, and BCC equivalents for reference by the reader during the following discussion.

The defining feature of any ideal quartz structure is perfectly regular tetrahedra. Ideal α-quartz has perfectly regular tetrahedra and is completely determined when two parameters are specified—the Si-O-Si angle and the model oxygen radius. In other words, there is one ideal α-quartz geometry for a given Si-O-Si angle that is unique up to isotropic scaling of the structure, and the model oxygen radius determines the cell volume. Isotropic scaling of the structure can be thought of as representing isotropic bond compression or expansion, or, equivalently, as a decrease or increase in the model oxygen radius. Any parameters that have a one-to-one correspondence with the angle or the radius also can be used to calculate the structure. An important example is the *c/a* axial ratio, which is uniquely determined in an ideal α-quartz structure by the Si-O-Si angle and vice versa. There is also a one-to-one relationship between the Si-O-Si angle and the absolute value of the tetrahedral rotation angle (Fig. 2, see also Fig. 6), so geometric changes can equivalently be described in terms of Si-O-Si angle-bending or tetrahedral rotation. They are the same mechanism. Another important relationship is the bijection between model oxygen radius and volume for a given Si-O-Si angle in ideal quartz. The ideal equivalent to an observed α-quartz structure is defined as the ideal α-quartz with the same volume and Si-O-Si angle as its observed counterpart.

Ideal β-quartz has a geometry that is unique up to isotropic scaling of the structure, with an Si-O-Si angle of $\cos^{-1}[-(\sqrt{3} + 1)/3] = 155.6°$ and *c/a* axial ratio of $3/(\sqrt{3} + 1) = 1.098$. Thus, the model oxygen radius completely determines the structure. Ideal β-quartz is the endpoint structure that the ideal α-quartz in both the $\alpha1$ and $\alpha2$ settings converges upon as the Si-O-Si angle increases. For Si-O-Si angles greater than 155.6°, no ideal quartz with perfectly regular tetrahedra can exist. Because ideal β-quartz has a fixed Si-O-Si angle that differs from the measured angles in observed β-quartz structures (ideal is ~2–2.5 degrees larger), the ideal equivalent to an observed β-quartz is defined to be the ideal β-quartz with the same volume but not necessarily the same Si-O-Si angle.

Model quartz is defined as ideal α-quartz distorted by altering the axial ratio to match an observed quartz structure. This results in a specific kind of distortion to the tetrahedra, but allows the derivation of a model that very closely matches observed quartz. The model equivalent to an observed quartz structure has the same volume, Si-O-Si angle, and *c/a* ratio as its

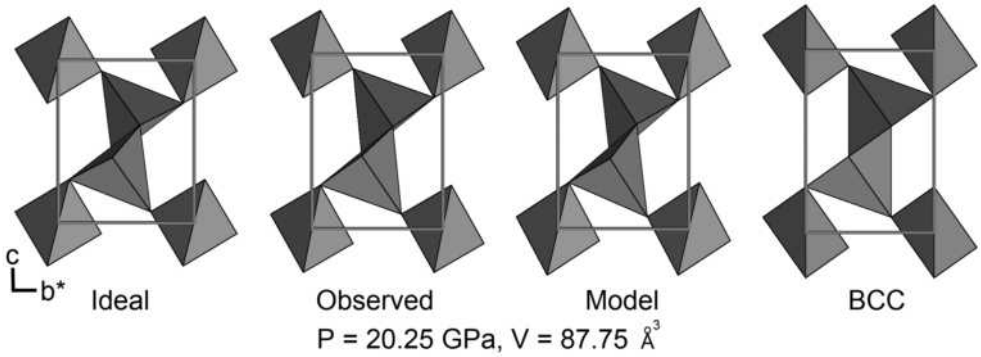

FIGURE 4. A comparison of observed quartz at 20.25 GPa (Dera et al. in prep) with three hypothetical structures with the same volume: ideal quartz, model quartz, and BCC quartz. Ideal quartz has regular tetrahedra and Si-O-Si angle equal to the observed, model quartz additionally has the same *c/a* axial ratio as observed.

observed counterpart. It is formed from an ideal quartz structure using only three mechanisms: tetrahedral rotation (Si-O-Si angle bending), alteration of the axial ratio, and isotropic scaling of the structure (equivalent to isotropic bond compression or expansion). The angle bending is necessary because altering the axial ratio alters the Si-O-Si angle, so a different initial ideal angle is needed to derive a model with the same angle as the observed equivalent. The model quartz concept is not extended to β-quartz in this paper because the axial ratio is fixed in ideal β-quartz and nearly so in observed β-quartz (Fig. 5).

BCC quartz has a perfectly body-centered cubic (BCC) arrangement of anions, and is described in detail in Thompson and Downs (2010). It is a hypothetical α-quartz that has a geometry that is unique up to isotropic scaling of the structure, with a fixed axial ratio of 1.225 and an Si-O-Si angle of 113.6°. The BCC equivalent to an observed quartz structure is defined as the BCC quartz with the same volume as its observed counterpart.

The observed quartz structures used in this paper for comparison with the models come from Kihara's (1990) high-temperature study, Glinnemann et al.'s (1992) high-pressure investigation, and Dera et al.'s (in prep) high-pressure investigation. Kihara's (1990) published data set is used with the exception of data points at 854, 859, and 869 K, which are considered redundant for our purposes. This is because Kihara (1990) recorded many data points to isolate the α-β transition and omitting the data points between 848 and 891 K reduces clutter in the figures without losing important information.

This paragraph presents a brief overview of the Dera et al. (in prep) very high-pressure experiment. Two micro-crystals of natural quartz with different orientations were loaded into a diamond anvil cell and single-crystal X-ray diffraction data was collected at the GSECARS facility at Advanced Photon Source, Argonne National Laboratory. Diffraction images were analyzed using the GSE_ADA/RSV software package. Standard deviations for the cell and positional parameters were less than 0.003 Å to the highest pressure. A separate publication will describe this experiment and present the resulting data in detail.

Because the hypothetical structures are not generated from experimental data but derived from exact equations, there is no error intrinsic to them. However, the hypothetical data presented in this paper were created using values for volume and, in some cases, Si-O-Si angle that were taken from observed structures

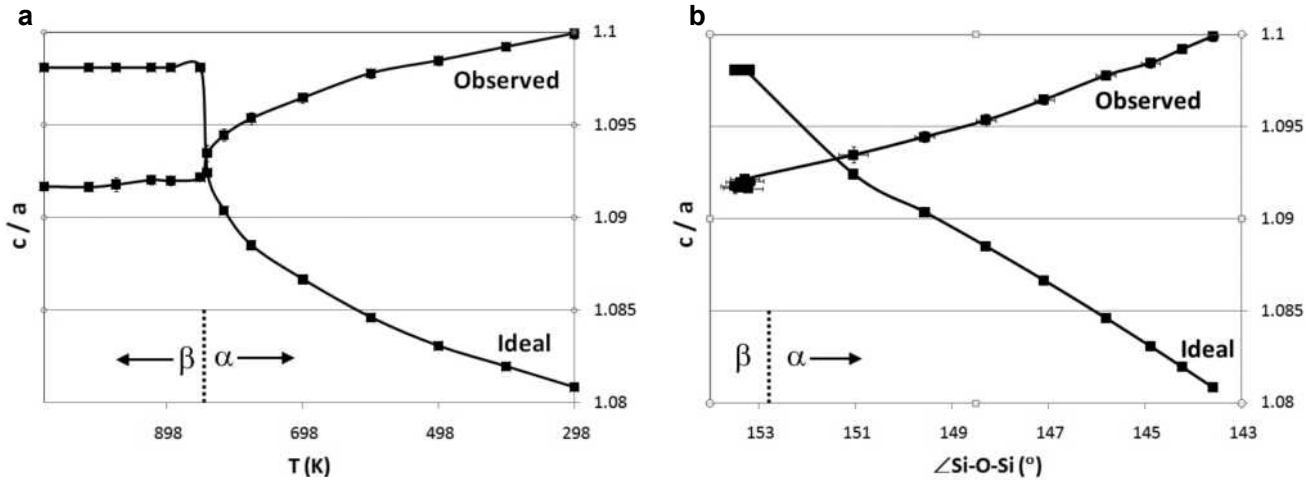

FIGURE 5. The *c/a* axial ratio for observed and ideal quartz plotted against (**a**) temperature and (**b**) Si-O-Si angle. This plot illustrates two points. First, that a parameter vs. temperature plot for β-quartz is often a horizontal line that collapses to a point in a parameter vs. angle plot. Second, that the *c/a* ratio for observed and ideal quartz is diverging as temperature decreases. All temperature error bars and some of the others are too small to be seen.

that do have errors associated with them. The hypothetical structures were calculated to match these values to a precision much greater than the precision of the observed quantities. It is reasonable to view the hypothetical structures as errorless abstract entities that exist independent of uncertainties introduced by experimental techniques. Table 1 summarizes the relationship between the various models and observed quartz. (Hypothetical Crystal Structures table is on deposit[1].)

Figure 5 illustrates an important point about interpreting the figures in this paper. Most of quartz's crystallographic parameters vary smoothly as a function of Si-O-Si angle whether the angle is changing because temperature is changing or because pressure is changing. Therefore, plotting a parameter of interest against the angle allows the pressure and temperature data sets to be neatly combined into one plot. However, this rule of thumb breaks down for β-quartz because the angle remains essentially constant above the transition temperature. So do most other crystallographic parameters. This has the effect of condensing a horizontal line in a parameter vs. temperature plot for β-quartz into a point in a parameter vs. angle plot. As an example, Figure 5 plots the axial ratio for β- and α-quartz at temperature (Kihara 1990) both ways. Figure 5a is the ratio vs. temperature plot and Figure 5b is the ratio vs. angle plot. Because of the "endpoint" nature of β-quartz, the behaviors of interest in this investigation are in the α-phase, and we have chosen the parameter vs. angle format for many of our plots to reduce their number and increase (hopefully) their clarity, focusing on the role of the Si-O-Si angle in the behavior of quartz under changing conditions of temperature and pressure. Plotting data in this manner demonstrates the inverse relationship between the effect of increasing temperature and increasing pressure typical of many crystalline materials (Hazen and Prewitt 1977).

IDEAL QUARTZ

This section presents crystallographic data for ideal quartz and highlights some of its interesting characteristics (derivation details are presented in the Appendix[1]). Ideal quartz is constrained to have perfectly regular tetrahedra. This means that ideal quartz can compress or expand through only two mechanisms—Si-O-Si angle-bending and isotropic scaling of the structure (i.e., isotropic bond compression or expansion, or, equivalently, changes in the model oxygen radius).

In quartz, observed and ideal, Si-O-Si angle-bending and tetrahedral rotation around **a** are equivalent mechanisms. Figure 6 illustrates the relationship between the tetrahedral rotation angle, ϕ, and the Si-O-Si angle, θ. The model oxygen radius is represented by "r". The relationship between ϕ and θ in ideal quartz is expressed mathematically by the equation (see Appendix for derivation):

$$\cos\phi = \sqrt{(-\cos\theta + 3/4)} - 1/(2\sqrt{3}).$$

[1] Deposit item AM-11-054, Appendix, Appendix Figures 1–7; Appendix Table (Hypothetical Crystal Structures). Deposit items are available two ways: For a paper copy contact the Business Office of the Mineralogical Society of America (see inside front cover of recent issue) for price information. For an electronic copy visit the MSA web site at http://www.minsocam.org, go to the *American Mineralogist* Contents, find the table of contents for the specific volume/issue wanted, and then click on the deposit link there.

TABLE 1. The relationship between several different models for quartz and their observed quartz equivalents

	Volume	Si-O-Si	**c/a**	Tetrahedra
Ideal β-quartz	equals observed	155.6°	1.098	regular
Ideal α-quartz	equals observed	equals observed	f(∠Si-O-Si)†	regular
Model α-quartz	equals observed	equals observed	equals observed	distorted
BCC quartz	equals observed	113.6°	1.225	Sommerville*

* See Thompson and Downs (2010) for a detailed description of Sommerville tetrahedra.
† See text.

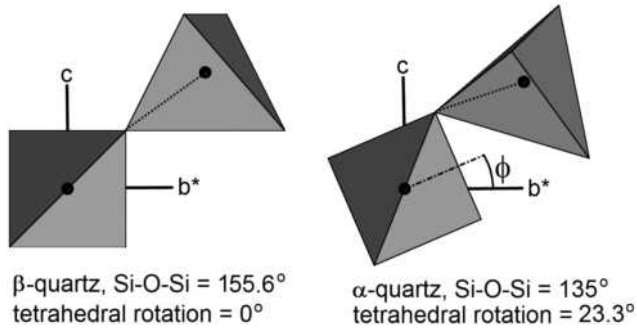

FIGURE 6. The relationship between the tetrahedral rotation angle, ϕ, and the Si-O-Si angle, θ. Ideal β-quartz has a rotation angle of 0° and an Si-O-Si angle of 155.6°. An ideal α-quartz is also illustrated with a rotation angle of 23.3° and an Si-O-Si angle of 135°.

This equation determines the domain of θ values over which ideal quartz can exist. Equations for the cell and positional parameters in an ideal quartz structure with given ϕ are:

$$a = r(\sqrt{6}\cos\phi + \sqrt{2})$$
$$c = 3\sqrt{2}r\cos\phi$$
$$x_O = \{-\sqrt{2}r[(\cos\phi/\sqrt{3}) + 1]/a\} + 1$$
$$y_O = \{-\sqrt{2}r[(2\cos\phi/\sqrt{3}) - (\sin\phi/\sqrt{3}) + 1]/a\} + 1$$
$$z_O = r[\sin(\phi + 45°)/c - 1/3]$$
$$x_{Si} = (x_O - 2y_O + 2)/4.$$

The significant difference between observed and ideal quartz is the *c/a* axial ratio. Figure 7 plots *c/a* for observed, ideal, and BCC quartz (model quartz has the same ratio as observed). The figure shows that as the Si-O-Si angle decreases from 153 to 125°, *c/a* in observed quartz increases from 1.09 to 1.15 and that the rate of change of *c/a* increases as the angle gets smaller. The axial ratio is moving toward the limiting BCC value of *c/a* = 1.22°. This is opposite to the behavior of ideal quartz, whose axial ratio decreases from 1.10 to 1.04 over the same domain. Since deviation from the ideal axial ratio is not necessary for quartz to compress, why does it happen? Possible forces opposing maintenance of the ideal ratio as quartz compresses and the Si-O-Si angle decreases are anion-anion repulsion and cation-cation repulsion. Figure 8 is a plot of the shortest intertetrahedral Si-Si and O-O separations in quartz between 0.59 and 20.25 GPa (Dera et al. in prep), for both observed and ideal. It shows essentially no deviation between observed and ideal R(Si-Si) but dramatically larger observed R(O-O) than ideal, with the difference increasing as pressure increases. This is consistent with the hypothesis that anion-anion repulsion is an important interaction in quartz as it compresses and that cation-cation repulsion has little, if any, effect.

Comparison of observed quartz with the hypothetical structures

To quantitatively compare observed quartz with ideal, model, and BCC quartz, a parameter, U_{qtz}, has been derived that quantifies the difference between two quartz structures. It is a measure of the mean squared displacement of 864 atoms in one quartz structure (a $4 \times 6 \times 4$ block of unit cells) from their corresponding atoms in a second quartz structure: $U_{qtz} = \Sigma_{i=864}$ $[R_i^2(atom_{qtz1}\text{-}atom_{qtz2})/864]$, where R_i is the distance from the i^{th} atom in the first structure to its equivalent in the second structure. The fit between the two atomic arrangements is accomplished by rotating and translating the arrangements relative to each other until U_{qtz} is minimized. A U_{qtz} value of zero is a perfect match, i.e., the structures are identical. A value of one means that the two structures are very different from one another, so the mismatch between quartz structures increases as U_{qtz} increases. Alternatively, one can think of the match or fit as improving as U_{qtz} decreases. A similar parameter for analyzing cubic-closest packing and hexagonal closest-packing efficiency is described in Thompson and Downs (2001), another parameter for comparing pyroxenes in Thompson and Downs (2008), and one more for analyzing BCC packing efficiency in quartz in Thompson and Downs (2010).

To avoid confusion between the calculation of the models and the calculation of U_{qtz}, this paragraph reviews the process of arriving at a value of U_{qtz} from the beginning. It begins with the calculation of a hypothetical quartz equivalent to a data set of interest for observed quartz. For BCC quartz, the atomic positions and cell parameter ratio are fixed (Thompson and Downs 2010). To create a BCC equivalent, the model oxygen radius of the BCC structure is varied in a simple computer program until the model volume matches the observed to a precision much greater than the error in the observed value. To derive an ideal equivalent, the equations given in the ideal quartz section are used to calculate the atomic positions and a starting set of cell parameters for the model. The model oxygen radius is then varied (which does not affect the cell parameter ratio) until the volume matches the observed crystal. A model equivalent is derived using the same equations and altering the cell parameter ratio to match the observed ratio. An additional step is required because altering the cell changes the Si-O-Si angle, so a starting angle is varied until the final angle matches. At this point, there is a hypothetical structure that fulfills a set of prescribed constraints and an observed structure with the same volume. Now U_{qtz} can be calculated using the procedure described in the preceding paragraph, which does not change either structure. It merely puts them in one coordinate system and alters their relative positions and orientations until the mean square displacement of their corresponding atoms is minimized. Other measures of similarity could have been invented, but we believe that this one is extremely robust.

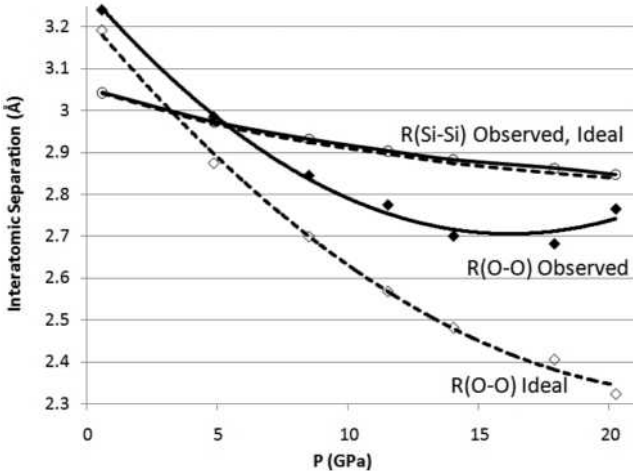

Figure 8. Interatomic separations for nearest neighbor Si-Si and intertetrahedral O-O interactions in ideal and observed quartz. This plot is consistent with O-O interactions being much more important in the behavior of quartz with pressure than Si-Si interactions.

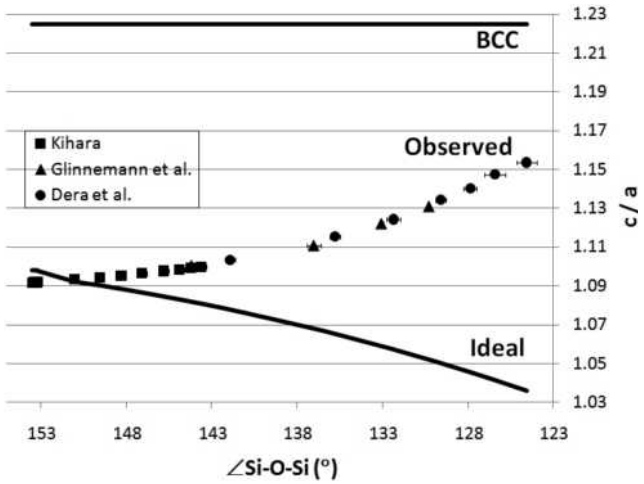

Figure 7. The *c/a* axial ratio vs. Si-O-Si angle for four structures: ideal quartz with perfectly regular tetrahedra, observed quartz (model quartz has the same ratio), and BCC quartz. All of the vertical error bars and some of the horizontal ones are too small to be seen.

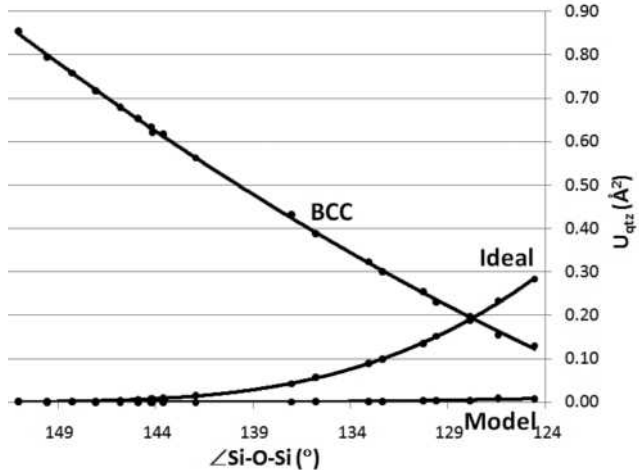

Figure 9. A comparison of three hypothetical structures with observed quartz. U_{qtz} is a measure of the similarity of one quartz structure to another. A value of 0 is an exact match (the structures are identical), while a value of 1 is a very poor fit. As Si-O-Si angle decreases, quartz is becoming more like BCC quartz and less ideal.

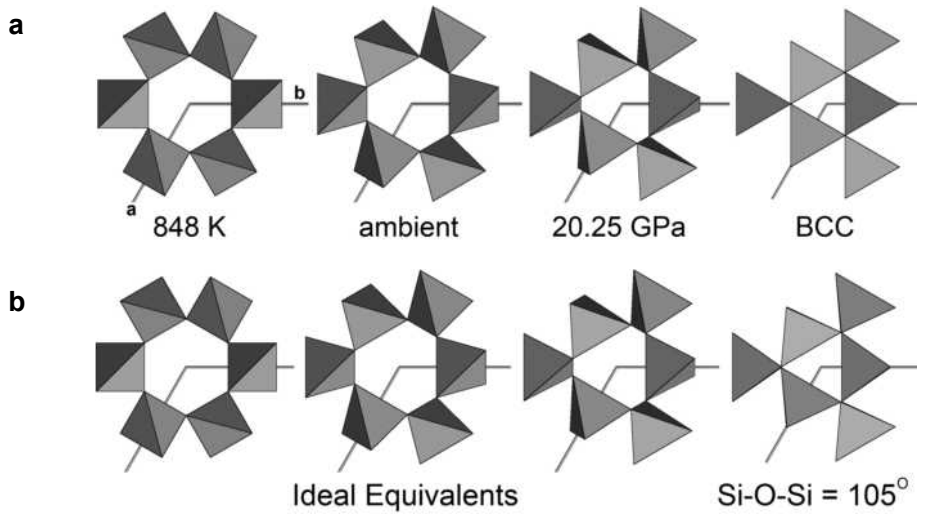

FIGURE 10. The collapse of the large channel in quartz as the Si-O-Si angle decreases in observed (**a**) and ideal (**b**) quartz. Quartz at 848 K is from Kihara (1990), room conditions is from Glinnemann et al. (1992), and 20.25 GPa is from Dera et al. (in prep). (**a**) has a cartoon of BCC quartz at the right end to provide visual evidence that quartz is trending toward BCC as temperature decreases/pressure increases. (**b**) shows that angle-bending in ideal quartz collapses the channel and that angle-bending and channel collapse are different descriptions of the same mechanism.

The algorithm for calculating U_{qtz} results in a parameter that is precise to many digits if given exact input. However, U_{qtz} cannot be more precise than its input and there is uncertainty in the observed quartz data sets. Nonetheless, the quality of the data sets and the robustness of the parameter are reflected in the very low scatter about the fitted curves in Figure 9.

Figure 9 compares the fit between ideal, model, BCC, and observed quartz. Quartz at high temperature is almost ideal (Si-O-Si is large). As temperature decreases and then pressure increases (Si-O-Si decreases), quartz becomes less and less ideal and more and more like BCC quartz. At 20.25 GPa (Si-O-Si = 124.6°), U_{qtz}(BCC quartz) = 0.13 and U_{qtz}(ideal quartz) = 0.28, so observed quartz is much more like BCC quartz than ideal quartz. Model quartz, created from ideal quartz by a combination of Si-O-Si angle-bending, alteration of the *c/a* axial ratio to match observed, and isotropic scaling to match observed volume, is a very good representation of observed quartz over the entire Si-O-Si domain of the analyzed experiments. While Figure 9 shows that model quartz is a very good match for observed quartz, it does not explain the deviation of the axial ratio from ideal seen in nature and built into the model. The next section will present evidence that the deviation in the axial ratio from ideal in observed quartz as Si-O-Si decreases is a result of quartz's increasing resemblance to BCC quartz as pressure increases, and therefore the result of anion-anion repulsion.

COMPRESSION MECHANISM OF QUARTZ

The principal compression mechanism of quartz can be described as the collapse of the large channel centered on the **c**-axis, noted by d'Amour et al. (1979). Figure 10a shows this collapse in observed quartz as temperature decreases/pressure increases. BCC quartz has been added on the right of Figure 10a as visual evidence of our assertion that this is the end-member hypothetical structure that quartz is trending toward as pressure increases. Bond compression provides only a small contribution (Levien et al. 1980), and Thompson and Downs (2010) have argued that tetrahedral distortion should not be considered a compression mechanism. The channel collapse compression mechanism of quartz is equivalent to the Si-O-Si angle-bending/tetrahedral rotation mechanism, which also collapses the channel. This is illustrated in Figure 10b, which shows the collapse of the channel in ideal quartz as it compresses through angle-bending and isotropic scaling alone. Channel collapse and angle-bending are different descriptions of the same mechanism.

d'Amour et al. (1979) attributed the shrinking cross section of the quartz channel to the increasing *c/a* axial ratio with pressure. However, Figure 10b shows that Si-O-Si angle-bending in ideal quartz collapses the channel just as effectively as is observed in real quartz, and *c/a* decreases in ideal quartz as the angle bends. Therefore, the deviation from ideal of the axial ratio in observed quartz must be caused by something other than channel collapse.

Model quartz (not ideal) is now compared to observed quartz because model quartz is ideal quartz altered by arbitrary changing of the axial ratio to match observed. Therefore, the differences between observed quartz and model [which must be subtle (Fig. 9) and do not include the axial ratio] may provide an explanation for the axial ratio that is not arbitrary.

Figure 11 is a plot of intrafacial angle variance (Thompson and Downs 2010) for observed quartz (Dera et al. in prep) and model quartz at high pressure. Intrafacial angle variance is a cation-independent measure of the similarity of the Si tetrahedron to the BCC tetrahedron, called a Sommerville tetrahedron (O'keeffe and Hyde 1996). An angle variance of zero means that a tetrahedron is a Sommerville tetrahedron, while larger values of the variance indicate increasing distortion from a BCC tetrahedron. Figure 11 shows that the Si tetrahedron in observed quartz becomes steadily more like a BCC tetrahedron as pressure increases, while the model tetrahedron becomes slightly less like a Sommerville tetrahedron. This indicates that while model quartz is a very good representation of observed quartz, it fails to capture some subtle details of real quartz that reflect the forces that drive the behavior of quartz with pressure.

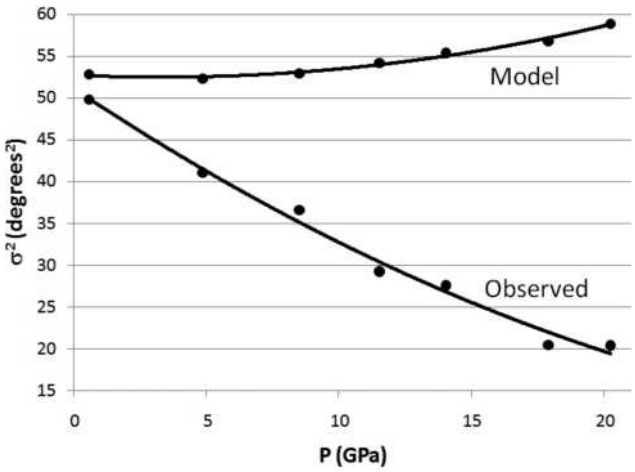

FIGURE 11. The similarity to the BCC tetrahedron in observed and model quartz. Intrafacial variance (Thompson and Downs 2010) is a cation-independent measure of the fit between a tetrahedron and the BCC Sommerville tetrahedron (O'Keeffe and Hyde 1996). The Si-tetrahedron in observed quartz is becoming more like the BCC tetrahedron as pressure increases, while the tetrahedron in model quartz is diverging from BCC.

Careful comparison of the observed and model tetrahedra in Figure 4 reveals that the corner angles of the projection of the tetrahedra centered on the **a**-axis into the **b*c**-plane are closer to 90° than those of the projection of the model. This is because this angle in the projections of both regular and Sommerville (BCC) tetrahedra is 90°, and the angle in real quartz does not deviate far from the angle in these hypothetical endpoint structures. Thus, arbitrary alteration of the model axial ratio to match the observed ratio results in a model that does not incorporate some of the details that reflect the fact that anion-anion repulsion is driving quartz toward a BCC arrangement of the oxygen anions as pressure increases. Therefore, the distortion in the model tetrahedra from regular is different than the very specific distortion that occurs in BCC quartz and that is also seen in observed quartz as pressure increases.

Ideal and BCC quartz can be considered hypothetical low-pressure and high-pressure endpoint structures for α-quartz, respectively. At room conditions, ideal quartz very closely approximates α-quartz (Fig. 9). However, as pressure increases, quartz becomes less and less ideal, and more and more like BCC quartz. Ideal quartz could theoretically compress as effectively as real quartz (Fig. 1), but as the volume of observed quartz decreases, anion-anion distances decrease and repulsion increases, forcing changes in the structure that maximize the minimum anion-anion separations. The need to reduce volume and the need to maintain anion separation are competing forces in quartz as pressure increases. Combined, these two needs result in the changes that are observed in experiments. The need to reduce volume decreases the Si-O-Si angle, collapsing the large channel centered on **c**. The need to maintain anion separation forces the anions to adopt a more perfectly BCC arrangement, increasing the *c/a* axial ratio and distorting the Si tetrahedron from regular.

ACKNOWLEDGMENTS

Part of this work was performed at GeoSoilEnviroCARS (Sector 13), Advanced Photon Source (APS), Argonne National Laboratory. GeoSoilEnviro-CARS is supported by the National Science Foundation-Earth Sciences (EAR-0622171) and Department of Energy-Geosciences (DE-FG02-94ER14466). Use of the Advanced Photon Source was supported by the U.S. Department of Energy, Office of Science, Office of Basic Energy Sciences, under Contract No. DE-AC02-06CH11357.

Robert T. Downs gratefully acknowledges support from Carnegie-DOE Alliance Center under cooperative agreement DE-FC52-08NA28554.

REFERENCES CITED

Bragg, L., Claringbull, G.F., and Taylor, W.H. (1965) Crystal Structures of Minerals. Cornell University Press, Ithaca, New York.

d'Amour, H., Denner, W., and Schulz, H. (1979) Structure determination of α-quartz up to 68×10^8 Pa. Acta Crystallographica B35, p. 550–555.

Deer, W.A., Howie, R.A., and Zussman, J. (1978) Rock-Forming Minerals, Volume 2A, Second Edition, Single Chain Silicates. Wiley, New York.

Dove, M.T., Heine, V., and Hammonds, K.D. (1995) Rigid unit modes in framework silicates. Mineralogical Magazine, 59, 629–639.

Glinnemann, J., King, H.E. Jr., Schulz, H., Hahn, Th., La Placa, S.J., and Dacol, F. (1992) Crystal structures of the low-temperature quartz-type phases of SiO_2 and GeO_2 at elevated pressure. Zeitschrift für Kristallographie, 198, 177–212.

Hazen, R.M. and Prewitt, C.T. (1977) Effects of temperature and pressure on interatomic distances in oxygen-based minerals. American Mineralogist, 62, 309–315.

Kihara, K. (1990) An X-ray study of the temperature dependence of the quartz structure. European Journal of Mineralogy, 2, 63–77.

Levien, L., Prewitt, C.T., and Weidner, D.J. (1980) Structure and elastic properties of quartz at pressure. American Mineralogist, 65, 920–930.

Megaw, H. (1973) Crystal Structures: A working approach, 249 p. Saunders, Philadelphia.

O'Keeffe, M. and Hyde, B.G. (1996) Crystal Structures Volume 1: Patterns and Symmetry. Monograph, Mineralogical Society of America, Chantilly, Virginia.

Robinson, K., Gibbs, G.V., and Ribbe, P.H. (1971) Quadratic elongation: a quantitative measure of distortion in coordination polyhedra. Science, 172, 567–570.

Ross, N.L. (2000) Framework structures. In R.M. Hazen, and R.T. Downs, Eds., High-Temperature and High-Pressure Crystal Chemistry, 41, p. 257–287. Reviews in Mineralogy and Geochemistry, Mineralogical Society of America, Chantilly, Virginia.

Smith, G.S. (1963) On the regularity of the tetrahedra in quartz. Acta Crystallographica, 16, 542–545.

Sowa, H. (1988) The oxygen packings of low-quartz and ReO_3 under high pressure. Zeitschrift für Kristallographie, 184, 257–268.

Taylor, S.R. and McLennan, S.M. (1985) The Continental Crust: its Composition and Evolution. Blackwell Scientific Publications, Oxford.

Thompson, R.M. and Downs, R.T. (2001) Quantifying distortion from ideal closest-packing in a crystal structure with analysis and application. Acta Crystallographica, B57, 119–127.

——— (2008) The crystal structure of diopside at pressure to 10 GPa. American Mineralogist, 93, 177–186.

——— (2010) Packing systematics of the silica polymorphs: The role played by oxygen-oxygen nonbonded interactions in the compression of quartz. American Mineralogist, 95, 104–111.

Young, R.A. (1962) Mechanism of the Phase Transition in Quartz. Air Force Office of Scientific Research, Washington, D.C.

MANUSCRIPT RECEIVED MARCH 26, 2011
MANUSCRIPT ACCEPTED JUNE 14, 2011
MANUSCRIPT HANDLED BY G. DIEGO GATTA

Deposit AM-11-054

The compression pathway of quartz

Richard M. Thompson, Robert T. Downs, and Przemyslaw Dera

Appendix

This appendix presents the derivation of the ideal quartz structures. All tetrahedra are perfectly regular with edge length 2r. Appendix Figure 1[1] illustrates an important quantity in the derivations. The dashed line segment, *h*, passing through the center of the tetrahedron is the portion of the tetrahedral twofold within the tetrahedron, and has length $\sqrt{2}r$. Alternatively, it can be described as the line segment connecting the midpoints of opposing tetrahedral edges.

Ideal β-quartz is relatively easy to derive. Appendix Figure 2 illustrates its unit cell. $\mathbf{c} = 3h = 3\sqrt{2}r$ and $\mathbf{a} = w + h = (\sqrt{6} + \sqrt{2})r$. Appendix Figure 3 allows the derivation of the oxygen x-coordinate. Because O is on a special position, $x_{O3} = x_{O1}/2$, so $x_m = 3x_{O1}/4$, and $x_{Si} = 1/2$, so $(1/2 - 3x_{O1}/4)/(3x_{O1}/4) = (\sqrt{2}/2)/(\sqrt{6}/2)$, giving $x_{O1} = 1 - 1/\sqrt{3}$.

Ideal α-quartz is more complicated. Coordinates for O2 (Appendix Fig. 3) are derived below in terms of a series intermediate parameters illustrated in Appendix Figure 4 and 6 and ultimately in terms of the tetrahedral rotation angle, ϕ, and the model oxygen radius, *r*. From this, the coordinates can be recast in terms of the Si-O-Si angle, θ, and used to calculate the position of O1 and Si

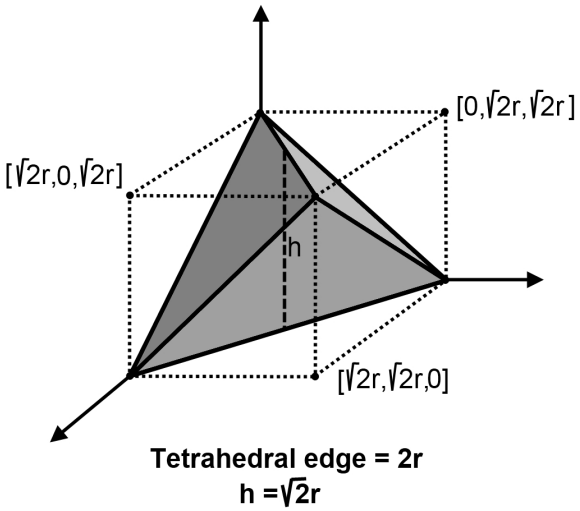

Appendix Figure 1. Tetrahedral geometry. The line segment, h, connecting the midpoints of opposing edges in a regular tetrahedron with edge length 2r has length $\sqrt{2}r$.

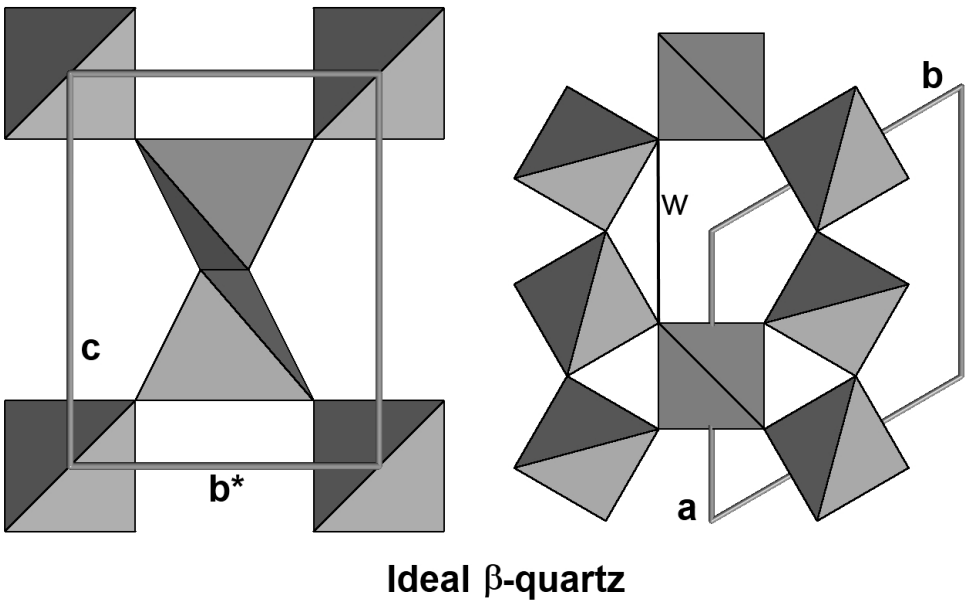

Appendix Figure 2. Cell parameters of ideal β-quartz. $c = 3\sqrt{2}r$, $a = \sqrt{6}r$.

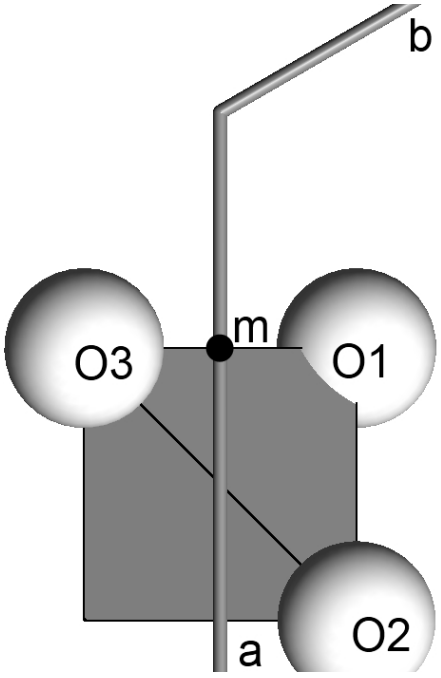

Appendix Figure 3. Deriving the oxygen x-coordinate of ideal β-quartz.

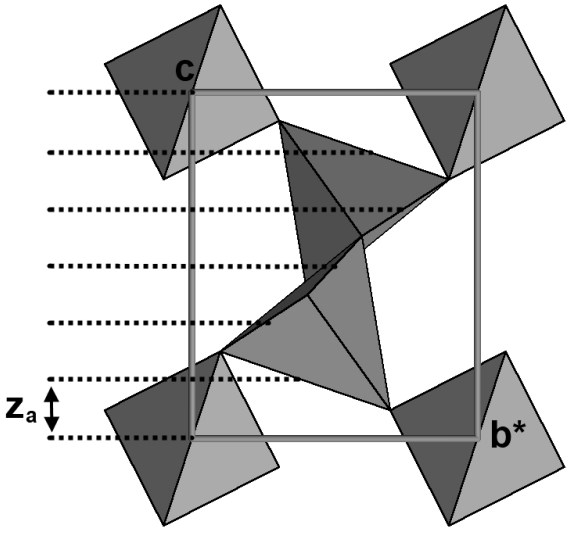

Appendix Figure 5. Deriving the c cell edge of ideal α-quartz. Each dotted line passes through the midpoints of the edges of tetrahedra. Thus, the same vertical percentage of each tetrahedron is between dotted lines and c = 6za.

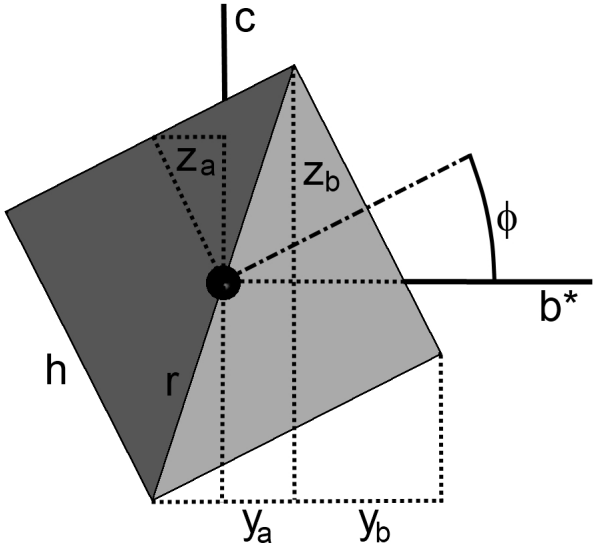

Appendix Figure 4. Deriving the oxygen positional coordinates of ideal α-quartz. za represents the length of the vertical line segment forming the right-hand side of the dotted triangle. zb represents the length of the dotted vertical line segment originating at and perpendicular to the ab-plane and ending at the uppermost corner of the tetrahedron. The ideal quartz structure in this example has an Si-O-Si angle of 130° and a tetrahedral rotation angle, φ, of 26.9°.

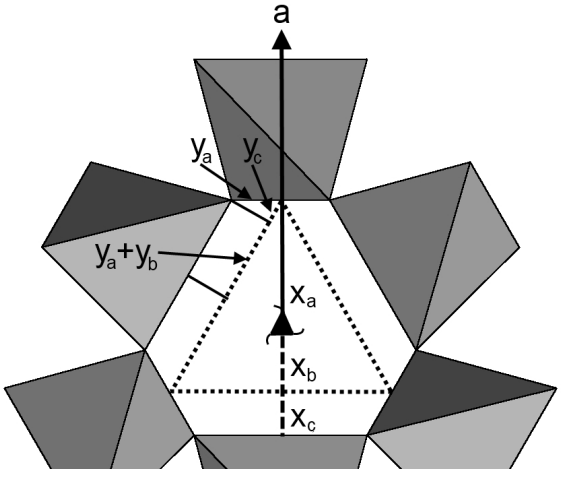

Appendix Figure 6. Important quantities in deriving a, xO2, and yO2. This ideal quartz structure in this example has an Si-O-Si angle of 145° and a tetrahedral rotation angle, φ, of 15.4°.

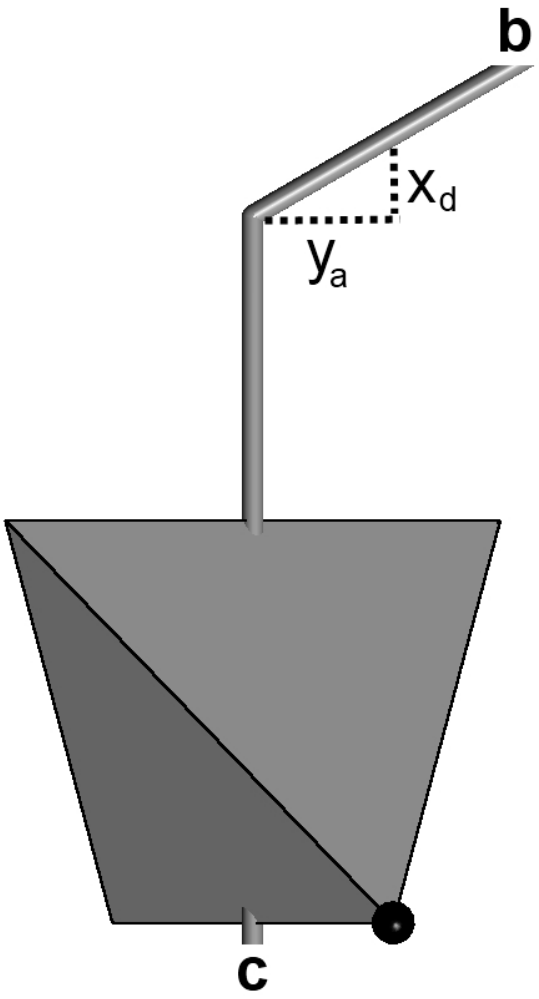

Appendix Figure 7. Deriving xO2 and yO2.

(see text). From Appendix Figure 4:

$h = \sqrt{2}r$
$z_a = r \cdot \cos\phi/\sqrt{2}$
$z_b = r \cdot \sin(\phi + 45°)$

by inspection of Appendix Figure 5, $c = 6z_a$

$z_{O2} = z_b/c$
$y_a = r \cdot \cos(\phi + 45°)$
$y_b = h \cdot \cos\phi - 2y_a = \sqrt{2}r \cdot \cos\phi - 2r \cdot \cos(\phi + 45°) = \sqrt{2}r \cdot \sin\phi.$

From Appendix Figure 6:

$y_c = y_a/2$
$x_a = (2/\sqrt{3}) \cdot (y_a + y_b + y_c)$
$x_b = x_a/2$
$x_c = (\sqrt{3}/2) \cdot y_a$
$a = x_a + x_b + x_c + h.$

From Appendix Figure 7:

$y_{O2} = (2y_a/\sqrt{3})/a$
$x_{O2} = (x_b + x_c + x_d + h)/a.$

Finally:

$x_{Si} = (x_{O2} + y_{O2} + 1)/4$
$x_{O1} = -x_{O2} + y_{O2} + 1$
$y_{O1} = -x_{O2} + 1$
$z_{O1} = z_{O2} - 1/3.$

To derive the relation between ϕ and the Si-O-Si angle, θ, examine the oxygen atom O2 at [*x, y, z*]. Form the vectors $\mathbf{v} = O2Si1$ and $\mathbf{w} = O2Si2$, where Si1 = [$(x + y + 1)/4$, 0, 0] and Si2 = [1, $(x + y + 1)/4$, 1/3]. Solve the equation $\cos\theta = \mathbf{v} \bullet \mathbf{w}/(||v|| \, ||w||)$, substitute the expressions for *x, y*, and *z* as functions of ϕ, and complete the square.

type	observed equivalent	condition	a	c	x(Si)
ideal alpha	Glinneman et al. (1992)	0 GPa	4.9494	5.3544	0.46988
ideal alpha	Glinneman et al. (1992)	4.0 GPa	4.8382	5.1670	0.45890
ideal alpha	Glinneman et al. (1992)	7.2 GPa	4.7676	5.0487	0.45308
ideal alpha	Glinneman et al. (1992)	10.2 GPa	4.7165	4.9616	0.44900
ideal alpha	Kihara (1990)	298 K	4.9425	5.3420	0.46896
ideal alpha	Kihara (1990)	398 K	4.9469	5.3523	0.46999
ideal alpha	Kihara (1990)	498 K	4.9530	5.3644	0.47105
ideal alpha	Kihara (1990)	597 K	4.9583	5.3778	0.47258
ideal alpha	Kihara (1990)	697 K	4.9658	5.3961	0.47476
ideal alpha	Kihara (1990)	773 K	4.9732	5.4133	0.47690
ideal alpha	Kihara (1990)	813 K	4.9790	5.4289	0.47927
ideal alpha	Kihara (1990)	838 K	4.9857	5.4465	0.48225
ideal beta	Kihara (1990)	848 K	4.9875	5.4767	0.5
ideal beta	Kihara (1990)	891 K	4.9880	5.4772	0.5
ideal beta	Kihara (1990)	920 K	4.9880	5.4772	0.5
ideal beta	Kihara (1990)	972 K	4.9881	5.4774	0.5
ideal beta	Kihara (1990)	1012 K	4.9866	5.4757	0.5
ideal beta	Kihara (1990)	1078 K	4.9868	5.4759	0.5
ideal alpha	Dera et al. (in prep)	0.59 GPa	4.9190	5.3019	0.46636
ideal alpha	Dera et al. (in prep)	4.87 GPa	4.8065	5.1203	0.45709
ideal alpha	Dera et al. (in prep)	8.51 GPa	4.7388	5.0098	0.45201
ideal alpha	Dera et al. (in prep)	11.53 GPa	4.6962	4.9318	0.44800
ideal alpha	Dera et al. (in prep)	14.04 GPa	4.6619	4.8739	0.44547
ideal alpha	Dera et al. (in prep)	17.09 GPa	4.6248	4.8161	0.44335
ideal alpha	Dera et al. (in prep)	20.05 GPa	4.6076	4.7728	0.44059
model alpha	Glinneman et al. (1992)	0 GPa	4.9210	5.4163	0.46982
model alpha	Glinneman et al. (1992)	4.0 GPa	4.7750	5.3046	0.45891
model alpha	Glinneman et al. (1992)	7.2 GPa	4.6764	5.2475	0.45319
model alpha	Glinneman et al. (1992)	10.2 GPa	4.6040	5.2070	0.44922
model alpha	Kihara (1990)	298 K	4.9137	5.4047	0.46890
model alpha	Kihara (1990)	398 K	4.9209	5.4091	0.46993
model alpha	Kihara (1990)	498 K	4.9297	5.4151	0.47099
model alpha	Kihara (1990)	597 K	4.9384	5.4213	0.47251
model alpha	Kihara (1990)	697 K	4.9509	5.4285	0.47471
model alpha	Kihara (1990)	773 K	4.9628	5.4360	0.47685
model alpha	Kihara (1990)	813 K	4.9728	5.4425	0.47924
model alpha	Kihara (1990)	838 K	4.9841	5.4500	0.48224
model alpha	Dera et al. (in prep)	0.59 GPa	4.8807	5.3855	0.46630
model alpha	Dera et al. (in prep)	4.87 GPa	4.7332	5.2800	0.45712
model alpha	Dera et al. (in prep)	8.51 GPa	4.6424	5.2198	0.45215
model alpha	Dera et al. (in prep)	11.53 GPa	4.5770	5.1920	0.44825
model alpha	Dera et al. (in prep)	14.04 GPa	4.5289	5.1643	0.44580
model alpha	Dera et al. (in prep)	17.09 GPa	4.4776	5.1379	0.44378
model alpha	Dera et al. (in prep)	20.05 GPa	4.4451	5.1283	0.44114

x(O)	y(O)	z(O)
0.41640	0.26843	-0.11845
0.41106	0.28773	-0.10001
0.40759	0.29764	-0.08992
0.40491	0.30444	-0.08270
0.41601	0.27009	-0.11692
0.41644	0.26824	-0.11863
0.41687	0.26634	-0.12037
0.41746	0.26358	-0.12287
0.41825	0.25960	-0.12644
0.41896	0.25569	-0.12990
0.41968	0.25129	-0.13374
0.42047	0.24573	-0.13852
0.42265	0.21132	-0.16667
0.42265	0.21132	-0.16667
0.42265	0.21132	-0.16667
0.42265	0.21132	-0.16667
0.42265	0.21132	-0.16667
0.42265	0.21132	-0.16667
0.41486	0.27471	-0.11261
0.41003	0.29084	-0.09690
0.40691	0.29943	-0.08805
0.40421	0.30610	-0.08091
0.40240	0.31027	-0.07632
0.40083	0.31372	-0.07244
0.39870	0.31816	-0.06733
0.41637	0.26855	-0.11834
0.41107	0.28771	-0.10003
0.40766	0.29745	-0.09011
0.40505	0.30408	-0.08309
0.41599	0.27019	-0.11683
0.41642	0.26835	-0.11853
0.41685	0.26645	-0.12027
0.41744	0.26369	-0.12277
0.41823	0.25971	-0.12635
0.41895	0.25578	-0.12983
0.41967	0.25136	-0.13369
0.42047	0.24576	-0.13851
0.41484	0.27481	-0.11252
0.41005	0.29078	-0.09696
0.40700	0.29920	-0.08829
0.40439	0.30569	-0.08136
0.40265	0.30972	-0.07693
0.40115	0.31302	-0.07323
0.39913	0.31728	-0.06836